Polymer Chemistry

ROYAL SOCIETY OF CHEMISTRY

PAPER

View Article Online
View Journal | View Issue

Check for updates

Cite this: *Polym. Chem.*, 2024, **15**, 1862

Polysarcosine functionalised cationic polyesters efficiently deliver self-amplifying mRNA†

Hulya Bayraktutan, [a] Rafał J. Kopiasz, [a,b] Amr Elsherbeny, [a] Magda Martinez Espuga,[c] Nurcan Gumus, [a] Umut Can Oz, [a,d] Krunal Polra,[e] Paul F. McKay, [e] Robin J. Shattock,[e] Paloma Ordóñez-Morán,[f] Alvaro Mata, [c,g] Cameron Alexander [a] and Pratik Gurnani *[h]

Messenger RNA (mRNA) technology is a potent platform for new vaccines and therapeutics. To deliver RNA medicines effectively, safe delivery vectors are crucial. Among these, poly(β-amino ester)s (PBAEs) complexes with nucleic acids have been shown as promising alternatives to conventional lipid nanoparticles, but toxicity and colloidal stability concerns still remain. Conjugation of poly(ethylene glycol) (PEG) has been used to mitigate these issues, but challenges associated with PEG-induced reactogenicity have emerged. Polysarcosine (pSar) has shown promise as a PEG alternative, demonstrating reduced reactogenicity when incorporated into lipid nanoparticles. We therefore developed a synthetic route to conjugate pSar on to PBAE end-groups, resulting in a pSar-PBAE-pSar triblock copolymer. Polyplexes containing various ratios (0, 20, 50, 80, 100% pSar) of the pSarylated and a non-pSarylated PBAE were prepared with self-amplifying messenger RNA, to examine the effect of surface pSar density. RNA encapsulation efficiencies, formulation properties and gene transfectability *in vitro* were then assessed indicating complete encapsulation of the cargo and sub-200 nm particle diameters in all cases. Despite high gene transfection in HEK293T cells, only the 50%-pSar displayed significantly higher expression of the reporter gene than the negative control in Caco-2. Further evaluation of 50%-pSar was conducted using 3D human colorectal cancer organoids, which displayed high transfection ability within the core of the organoid indicating high penetration of these nanoparticles. As a result, these findings indicate that pSarylated PBAEs have the potential to serve as a promising component material for enhancing delivery of nucleic acid therapeutics.

Received 18th January 2024,
Accepted 6th April 2024

DOI: 10.1039/d4py00064a

rsc.li/polymers

Open Access Article. Published on 11 abril 2024. Downloaded on 15/09/2024 5:24:48.
This article is licensed under a Creative Commons Attribution 3.0 Unported Licence.

Introduction

Messenger RNA (mRNA) technology is now recognised as a versatile and potent medicinal platform that enables the transient expression of selective proteins either as vaccines against infectious disease, or therapeutics for a range of indications, including genetic disorders, and cancer.[1,2] The successful demonstration of safety and efficacy for Moderna (SpikeVax) and BioNTech-Pfizer's (Comirnaty) mRNA-based vaccines against COVID-19, has significantly accelerated this technology, with many more mRNA vaccines and therapeutics now in clinical trials.[3]

One of the most important components of an effective RNA medicine is a safe and efficient delivery system to protect the genetic sequence from endogenous nucleases and facilitate translocation to the cytosol of the target cells for expression.[4–6] A variety of nonviral delivery strategies have therefore been investigated to deliver nucleic acids, including lipid nanoparticles (*e.g.* liposomes, cubosomes) and polyelectrolyte complexes (polyplexes).[3,7–9] Polyplexes are self-assemblies of

[a]*Division of Molecular Therapeutics and Formulation, Boots Science Building, School of Pharmacy, University of Nottingham, Nottingham, NG7 2RD, UK*
[b]*Warsaw University of Technology, Faculty of Chemistry, Noakowskiego 3 St., 00-664, Warsaw, Poland*
[c]*Division of Regenerative Medicine and Cell Therapies, BioDiscovery Institute, School of Pharmacy, University of Nottingham, Nottingham, NG7 2RD, UK*
[d]*Department of Pharmaceutical Technology, Faculty of Pharmacy, Ankara University, Ankara, 06560, Türkiye*
[e]*Department of Infectious Diseases, Section of Immunology of Infection, Imperial College London, Norfolk Place, London, W21PG, UK*
[f]*Centre for Cancer Sciences, BioDiscovery Institute, Translational Medical Sciences Unit, School of Medicine, University of Nottingham, Nottingham, NG7 2RD, UK*
[g]*Department of Chemical and Environmental Engineering, University of Nottingham, Nottingham, NG7 2RD, UK*
[h]*UCL School of Pharmacy, University College London, 29-39 Brunswick Square, Bloomsbury, London, WC1N 1AX, UK. E-mail: p.gurnani@ucl.ac.uk*
†Electronic supplementary information (ESI) available. See DOI: https://doi.org/10.1039/d4py00064a

This journal is © The Royal Society of Chemistry 2024

Open Access Article. Published on 11 abril 2024. Downloaded on 15/09/2024 5:24:48.
This article is licensed under a Creative Commons Attribution 3.0 Unported Licence.

positively charged polymers which condense negatively charged nucleic acids into small (50–200 nm) nanoparticles driven by opposing electrostatic interactions. One of the promising classes of polycations broadly tested as RNA delivery vectors are poly(β-amino ester)s (PBAE)s.[10,11] Due to ester bonds within the PBAEs' main chain, these polymers are readily biodegradable *via* hydrolysis, decreasing their potential long-term accumulation and enhancing RNA release.[12] These features, together with high flexibility of chemical functionality allowing for simple structural manipulation for a variety of nucleic acid types[13,14] render PBAE-based polyplexes prospective candidates for RNA formulations. However, the polycationic and hydrophobic nature of some specific sub-classes of PBAEs can result in cytotoxicity *via* membrane disruption, which has prevented their clinical application. Previous reports have shown that PBAEs coupled with poly(ethylene glycol) (PEG) exhibit decreased surface cationic charges when complexed with nucleic acids, and this can mitigate toxicity as well as decrease interactions with serum proteins.[15,16] Such an approach has been proven to prolong systemic circulation time of nanoparticles by shielding their surface from aggregation and phagocytosis and increase in-serum *in vitro* and *in vivo* transfection efficacy.[17–20]

Despite the popularity of PEG to confer "stealth" properties to nanoparticles in serum and the fact that PEG is classified as generally regarded as safe (GRAS)[15] there is a growing number of reports on strong reactogenicity induced by PEG or PEGylated drugs.[21] This issue has become more prevalent following the widespread use of PEGylated lipids within SpikeVax and Comirnaty COVID-19 vaccines, which have boosted pre-existing PEG antibody titers by up to 60-fold.[22] This creates an urgent need to develop PEG alternatives, as future mRNA therapeutics which include PEG components may be highly immunogenic, thereby reducing potency and tolerability.[23–25] One emerging PEG alternative is polysarcosine (pSar), a polypeptoid – a non-toxic, endogenous and non-proteinogenic amino acid which therefore endows it with key advantages over other potential "stealth" polymers such as poly(vinyl pyrrolidone)s,[26] polyphosphoesters,[27] polyglycerols,[28] polypeptides,[29] and poly(2-alkyl-oxazoline)s.[30] Despite pSar's polyamide backbone, there is no evidence for degradability of pSar under physiological conditions to its monomeric form of sarcosine, unlike its counterpart polypeptides. However, as pSar is commonly synthesised at low molar masses this enables clearance *via* renal filtration potentially alleviating the need for biodegradability.[31]

Despite the similar physicochemical properties to PEG, recent examples of polysarcosinylated lipid nanoparticles have shown colloidal stability and, importantly, substantially reduced immunogenicity compared to PEGylated derivatives.[32] However, to our knowledge pSar-PBAE conjugation has not been reported and may offer a versatile approach to a tuneable RNA delivery system combined with the advantages offered by pSar.

In this report, we demonstrate successful conjugation of pSar with a PBAE to yield a pSar-PBAE-pSar triblock copolymer (Fig. 1). To test application in an RNA delivery setting, the pSarylated PBAE was formulated with self-amplifying RNA, an alternative mRNA technology which includes replicase genes derived from the alphavirus genome within the construct. When saRNAs are translated, they not only express the encoded protein, but also cause replication of the RNA within the cytosol, enhancing protein expression levels at significantly lower doses, lengthening expression half-life and reducing the cost compared to mRNA.[8,33–35] The saRNA constructs were formulated into polyplexes with varying content of pSarylated and non-pSarylated PBAEs to evaluate the effect of pSar density. The *in vitro* tolerability and transfection efficiency of these blended pSarylated-PBAE polyplexes was then examined in two immortalised cell lines, (HEK293T and Caco-2). Finally, the cellular uptake and transfection efficiency in 3D human colorectal cancer organoids were investigated.

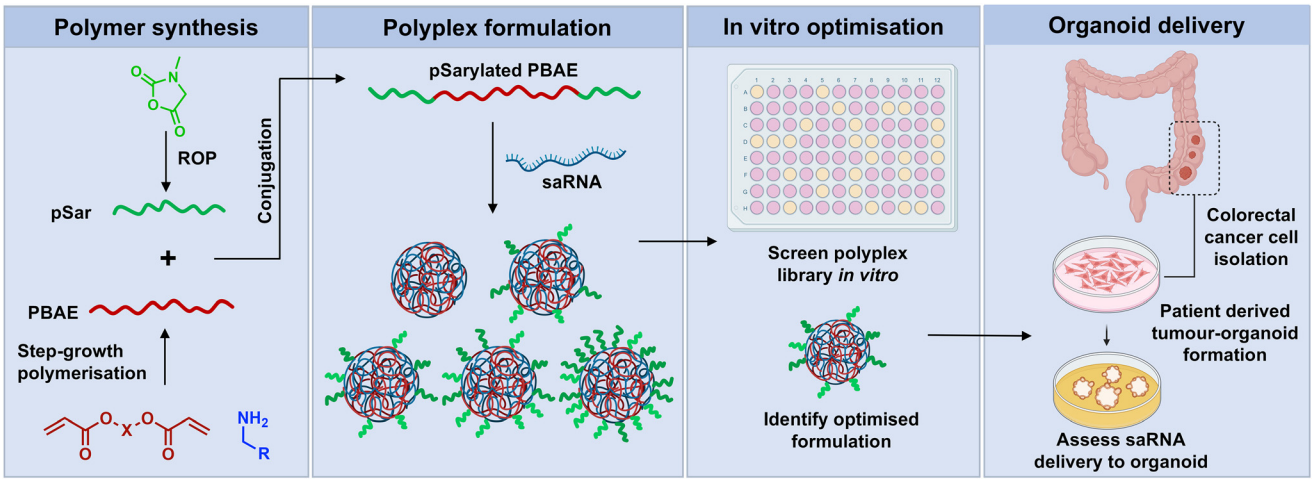

Fig. 1 Schematic representation of PBAE synthesis, polyplex assembly, *in vitro* analysis and the cellular uptake and transfection efficiency in 3D colorectal cancer organoids.

Open Access Article. Published on 11 abril 2024. Downloaded on 15/09/2024 5:24:48.
This article is licensed under a Creative Commons Attribution 3.0 Unported Licence.

Materials and methods

Materials

1,4-Butanediol diacrylate (BDD), 5-aminopentan-1-ol (5-AP), triethylamine (TEA), *N*-Boc-sarcosine, fluorescein isothiocyanate (FITC), diethyl ether, tetrahydrofuran, sodium acetate (NaOAc) buffer (pH: 5.0), dye gel red and goat-anti-mouse IgG, Fc biotin and red CellMask™ plasma membrane stain were purchased from Sigma-Aldrich. Dichloromethane (DCM), *N*,*N*-dimethylformamide (DMF), acetonitrile (ACN), tetrahydrofuran (THF), hexane, diethyl ether, dimethyl sulfoxide (DMSO), loading buffer, Tris-acetate-EDTA (TAE) buffer, tris-(2-hydroxyethyl)phosphine (THP), Lipofectamine Messenger MAX™, Hoechst 33342, Lysotracker red and 96-well plates were obtained from ThermoFisher. Dulbecco's modified Eagle's medium (DMEM) cell culture medium, RPMI 1640 cell culture medium, fetal bovine serum (FBS) and Opti-MEM were bought from Gibco, Invitrogen, Carlsbad, CA, USA. PrestoBlue reagent and ONE-Glo D-luciferin substrate were purchased from Promega, UK. HEK293T and Caco-2 cell lines were purchased from the ATCC.

Instrumentation and analysis

NMR spectroscopy. All ^{1}H-NMR spectra were recorded in ppm (δ) at 400 MHz in d_6-DMSO using a Bruker Avance III MHz spectrometer that was maintained at 25 °C. To analyse the spectra MestReNova 6.0.2 copyright 2009 (Mestrelab Research S.L.) was applied.

Gel permeation chromatography. The gel permeation chromatography (GPC) analysis was performed using the PL-50 instrument equipped with a dual angle light scattering (LS), viscometry (VS) and differential refractive index (DRI) detection system. The chromatography components were a PLgel 5 μm guard column and a 2× PLgel mixed D columns (300 × 7.5 mm). Dimethylformamide (DMF) with LiBr (0.1% wt/wt) was utilised as an eluent with a flow rate of 1 mL min^{-1} at 50 °C. The instrument was calibrated through poly(methyl methacrylate) standards (Agilent EasyVials) between 955 500–550 g mol^{-1}. Using conventional calibration, Cirrus GPC software, dispersity ($Đ$) values, molecular weight (M_w) and experimental molar mass (M_n, SEC) were measured.

DLS and zeta potential. A dynamic light scattering (DLS), Zetasizer nano-ZS90 (Malvern, Inc.), instrument was used to characterise the particles in terms of the size, PDI and zeta potential. The instrument was used at 25 °C to determine the zeta potential, average hydrodynamic diameters, and polydispersity index (PDI) of polyelectrolyte complexes.

Transmission electron microscopy. Briefly, glow discharged Formvar/carbon coated TEM grids were used, on which were placed the formulation samples (13 μL), which were left for 15 minutes, then the excess solution was removed and the samples allowed to dry at room temperature. Following this, 10 μL of 2% aqueous uranyl acetate was applied to each grid and left for 10 seconds. After air drying, imaging was performed using a Tecnai G2 Spirit TEM with BioTwin lens configuration (Thermo Fisher Scientific, Eindhoven, The Netherlands) at an accelerating voltage of 100 kV.

Polymer synthesis and characterisation

Sarcosine *N*-carboxyanhydride (SarNCA). A magnetically stirred solution of Boc-sarcosine (5.00 g, 26.5 mmol) and methyloxirane (18.5 mL, 265 mmol) in CH_3CN (100 mL) was cooled down in an ice bath and solid triphosgene (3.93 g, 13.5 mmol) was added in stepwise. Then, the reaction flask was half-closed to allow carbon dioxide to escape from the vessel. After 1.5 hours stirring at the ice bath, 50 mL of cold water was carefully added stepwise to quench the reaction. The mixture was extracted with ethyl acetate (2 × 100 mL), and the combined organic layers were washed with brine (2 × 100 mL), dried over anhydrous $MgSO_4$, and the solvent was removed using a rotatory evaporator. The obtained crude product was purified by recrystallization from hexane/THF at a freezer (−20 °C) yielding 2.10 g (69%) of white crystals. ^{1}H NMR (400 MHz, DMSO-d_6) δ 4.22 (s, 2H, –CH_2–), 2.87 (s, 3H, –CH_3); ^{13}C NMR (400 MHz, DMSO-d_6) δ 167.36, 152.59, 51.12, 29.79.

Cystamine. To a solution of cystamine hydrochloride (8.0 g, 35.8 mmol) in water (20 mL) a 10% w/w solution of $NaOH_{aq}$ (20 mL) was added and the mixture was stirred at room temperature for 15 minutes. Afterwards, it was extracted 3-times with DCM (3 × 30 mL), the organic phase was dried over $MgSO_4$ and concentrated on a rotatory evaporator yielding 4.2 g (78%) of a colourless oil.

^{1}H NMR (400 MHz, DMSO-d_6) δ 2.81 (t, J = 6.6 Hz, 4H, –CH_2-NH_2), 2.73 (t, J = 6.6 Hz, 4H, S-CH_2–), 2.20 (s, 4H, –NH_2); ^{13}C NMR (400 MHz, DMSO-d_6) δ 42.09, 41.28.

***N*,*N*-Bis(poly(sarcosine))-cystamine (pSar-cystamine).** To a solution of SarNCA (1.00 g, 8.7 mmol) in anhydrous DMF (3.2 mL) a solution of cystamine (36.7 mg, 0.24 mmol) in anhydrous DMF (2 mL) was added under argon atmosphere. After stirring overnight at room temperature, the product was isolated by precipitation in diethyl ether (80 mL) and purified by dissolving in MeOH (5 mL) and precipitation from diethyl ether (80 mL) two more times. The product was dried under vacuum overnight yielding 520 mg (80%) of white powder. Molecular weight determined by SEC: M_n = 3.1 kDa, M_w = 3.5, $Đ$ = 1.1; for ^{1}H NMR see spectrum S2 in ESI.†

pBDD-5AP. To 1,4-butanediol diacrylate (BDD, 1 g, 5.0 mmol) in DMSO (0.95 mL) 5-aminopentan-1-ol (5-AP, 470 mg, 4.59 mmol) in DMSO (2 mL) was added and the reaction was stirred at 90 °C overnight. Then, the mixture was diluted with THF (2.94 mL), the product was isolated by precipitation from diethyl ether (40 mL), and further purified by re-dissolving in THF (2 mL) and precipitation in diethyl ether (40 mL) thrice. The product was dried under vacuum overnight yielding 1250 mg (85%) of a yellowish oil. Molecular weight determined by SEC: M_n = 6.2 kDa, M_w = 8.0 kDa, $Đ$ = 1.3; for ^{1}H NMR see spectrum S1 in ESI.†

OH-(pBDD-5AP)-OH. To produce non-pSarylated PBAEs, an excess amount of 5-AP (260 mg, 0.26 mL, 2.52 mmol) was added to the pBDD-5AP (1000 mg, 5.04 mmol) in DMSO (5 mL) and the mixture was stirred for 24 hours at room temp-

 This journal is © The Royal Society of Chemistry 2024

Open Access Article. Published on 11 abril 2024. Downloaded on 15/09/2024 5:24:48.
This article is licensed under a Creative Commons Attribution 3.0 Unported Licence.

erature. Polymers were isolated by diluting the reaction mixture into THF (5 mL) followed by dropwise precipitation in diethyl ether (40 mL) thrice. The polymer was collected *via* centrifugation and dried under reduced pressure at 37 °C to yield 800 mg (80%) a yellow viscous liquid. Finally, polymers were stored at −20 °C as 100 mg mL^{-1} solution in DMSO. Molecular weight determined by SEC: M_n = 6.2 kDa, M_w = 13.5 kDa, $Đ$ = 2.1; for ^{1}H NMR see spectrum S4 in ESI.†

pSar-(pBDD-5AP)-pSar. pBDD-5AP (100 mg, 0.02 mmol), pSar-cystamine (108.1 mg, 0.07 mmol), triethylamine (2.27 mg, 3.13 μL, 0.02 mmol) and tris-(2-hydroxyethyl)phosphine (6.84 mg, 0.03 mmol) were added in DMF (4 mL) and the reaction was stirred at room temperature overnight. Then, the mixture was dialysed against DMF (1 L) for 30 hours and DMF solution was changed once. Afterwards, the mixture was precipitated in diethyl ether (40 mL) and to remove remaining DMF re-dissolved in methanol (2 mL) and was precipitated in diethyl ether (40 mL) twice. The product was dried under vacuum overnight yielding 85 mg (78%) of a sticky yellowish oil. Molecular weight determined by SEC: M_n = 7.6 kDa, M_w = 22.0 kDa, $Đ$ = 2.9; for ^{1}H NMR see spectrum S3 in ESI.†

Calculation of pSar theoretical molar masses from stoichiometry and NMR spectroscopy. Theoretical molar masses for pSar were calculated either from the polymerisation stoichiometry or from ^{1}H NMR analysis. Eqn (1) is used to calculate the theoretical number average molar mass ($M_{n,th}$), initial reaction stoichiometry, where $[M]_0$ and $[I]_0$ are the initial concentration (mol L^{-1}) of the SarNCA and cystamine bifunctional initiator respectively; p is the monomer conversion; and M_M and M_I are the molar mass of the monomer repeating unit and initiator respectively.

Calculation of the theoretical number average molar mass of

$$M_{n,th} = \frac{[M]_0 p M_M}{[I]_0} + M_I \quad (1)$$

An experimental number average molar mass from ^{1}H NMR spectroscopy $M_{n,NMR}$ can also be calculated using by dividing integrals of methyl signals for the sarcosine repeating units at 2.80 ppm (3H) and cystamine signals 3.70 ppm (2H).

Synthesis of fluorescently labelled polymers. BDD and BDD-pSAR polymers were dissolved in 5 mL DMSO (0.5 mg mL^{-1}) in a 20 mL vial. The dye FITC was added to the vials at a 1 : 10 (moles of end amine : FITC) molar ratio and triethylamine was added to the mixture at a 0.1 molar ratio to polymer. The reaction mixture was allowed to stir for 24 hours in the dark at room temperature. The reaction mixture was then dialysed in the dark using molecular weight cut-off 3.5 kDa against 250 mL NaOAc buffer (pH: 5.0). Purification was continued for 4 days and the dialysis medium refreshed 2 times in a day. After freeze drying, FITC-labelled polymers were collected as a yellow solid and were stored at −20 °C as 100 mg mL^{-1} solution in DMSO.

Polymer buffering capacity assay. The buffering capacity of pSarylated and non-pSarylated polymers was evaluated by acid–base titration over the pH range of 10.0–3.0. Briefly, 2 mg of polymer was dissolved in 30 mL of 0.1 M NaCl aqueous solution, and the solution was adjusted to pH 10.0 using 0.1 M NaOH. Then, precise volumes (between 10–20 μL) 0.1 M HCl were added until a pH of 3 was achieved. The pH after each addition of HCl was recorded. 0.1 M NaCl was set as negative control. The proton buffering capacity of polymers when pH is changed from 7.4 to 5.0 was calculated using equations below, where ΔV_{HCl} is the volume of $HCl_{(aq)}$ required to change pH from 7.4 to 5.0, [HCl] is the concentration of $HCl_{(aq)}$, which was 100 mM, m is the mass of the polymer, which was 2 mg, n was the moles of ionisable amines used in the titration, calculated from $M_{n,NMR}$ and DP of PBAE block.

Calculation of buffering capacity of polymer between pH 7.4 to 5.0 normalised to mass of polymer

$$\text{Buffering capacity(mass)} = \frac{\Delta V_{HCl}\,[HCl]}{m} \quad (2)$$

Calculation of buffering capacity of polymer between pH 7.4 to 5.0 normalised to moles of ionisable amines

$$\text{Buffering capacity(mol N)} = \frac{\Delta V_{HCl}\,[HCl]}{n} \quad (3)$$

Synthesis of saRNA

For firefly luciferase saRNA synthesis, luciferase encoded pDNA was linearised with Mlul-HF (NEB, UK) for 3 hours at room temperature. Uncapped RNA was synthesised in a MEGAscript reaction (Ambion, UK) using 1 μg of linearised DNA as a template. The RNA was then purified by LiCl precipitation (1 : 1 volume ratio) for 24 hours at −20 °C. Then, transcripts were centrifuged at 14 000 rpm at 4 °C for 20 minutes, washed once with 70% ethanol, centrifuged for 5 minutes, the ethanol wash was removed, and the pellet was dried at room temperature for 5 minutes. The purified RNA was then capped using ScriptCap Cap 1 capping system kit (CellScript, Madison, WI, USA) and used according to the manufacturer's protocol. Capped transcripts were again purified by LiCl precipitation. The purified capped saRNA was resuspended in RNAase/DNAase free water and stored at −80 °C at 800 μg mL^{-1}.

Preparation of polyplexes

Polyplexes were prepared by electrostatic interactions between positively charged polymers and negatively charged saRNA by mixing various w/w ratios (32, 64 and 128). Firstly, the working dilutions of polymers and saRNA were prepared in 25 mM NaOAc buffer (pH: 5.0). Depending on the desired w/w ratio, differing amounts of polymer stock solutions (100 mg mL^{-1} in DMSO) were mixed with nucleic acids in the buffer, gently mixed using a pipette and incubated at room temperature for 30 minutes. Whilst preparing the PBAE/saRNA complexes, taking a w : w 64 ratio as an example, 10 μg mL^{-1} of the RNA stock solution was mixed with 2.560 mg mL^{-1} PBAE by pipette using a 25 mM NaOAc buffer.

Open Access Article. Published on 11 abril 2024. Downloaded on 15/09/2024 5:24:48.
This article is licensed under a Creative Commons Attribution 3.0 Unported Licence.

Encapsulation efficiency determination using ribogreen assay

A fluorescence-based Quant-iT RiboGreen assay (ThermoFisher, UK) was utilised to be able to detect free RNA in solution after polymer encapsulation. Samples were diluted in 1× TE buffer (v/v 1 : 1) and the assay was performed according to the manufacturer's protocol. Samples were then loaded on a black, 96-well plate, and analysed for fluorescence on a microplate reader at an excitation of 485 nm and emission at 528 nm.

In vitro experiments

Cell culture. Cell line HEK293T was cultured in 10% (v/v) FBS containing high glucose DMEM cell culture medium. The human colon colorectal Caco-2 cell line was cultured in RPMI 1640 cell culture medium. Media used for cell culture studies contained L-glutamine and 10% FBS, and the absence of mycoplasma was confirmed using standard polymerase chain reaction assays. Cells were grown to 90% confluence in a humidified incubator at 37 °C, 5% CO_2 and detached with 1× trypsin/EDTA. Viability was assessed using Trypan blue staining.

Cell viability assays. To investigate the cytotoxicity of the formulations, a cell viability assay was performed in the HEK293T and Caco-2 cell lines. 24 hours prior to treatment, cells were seeded in a clear 96-well plate at a density of 20×10^3 cells per well. For the treatment, the medium was aspirated, and cells were treated with 200 μL of opti-MEM containing various w/w ratios of formulations complexed with 10 μg ml^{-1} fluc saRNA concentration (20 μL of polyplex solution). After 4 hours, nanoparticles were aspirated and 100 μL of complete medium was added to wells. At 24 hours posttreatment, each well was treated with 100 μL of 10% PrestoBlue reagent and allowed to incubate for 1 hour. Then, the total volume was transferred to a black 96-well plate and the FLUOstar Omega plate reader (BMG LABTECH, UK) was used to determine the fluorescent intensity (540 nm–590 nm) of each well and normalized to the medium control.

***In vitro* transfection experiments.** *In vitro* transfection experiments were performed in HEK293T and Caco-2 cell lines, and the commercially available transfection reagent Lipofectamine Messenger MAX™ was used as positive control. 24 hours prior to treatment, cells were seeded in a clear 96-well plate at a density of 20×10^3 cells per well. For the treatment, the medium was aspirated, then cells were transfected with 200 μL of Opti-MEM containing various w/w ratios of formulations complexed with 10 μg mL^{-1} fluc saRNA concentrations (20 μL of polyplex solution). After 4 hours, nanoparticles were aspirated and 100 μL of medium was added to wells. At 24 hours post-treatment, 50 μL of media was removed then 50 μL of the ONE-Glo D-luciferin substrate was placed into each well and mixed well by pipette. Finally, the total 100 μL was placed in a 96-well plate and FLUOstar Omega plate reader (BMG LABTECH, UK) was used to determine the luminescence.

Cellular uptake of saRNA using confocal microscopy. Caco-2 cells were seeded in CellView™ 35 mm diameter glass bottom cell culture dishes at a density of 30×10^4 cells per well. For the treatment, the medium was aspirated, and cells were transfected with Opti-MEM containing FITC labelled BDD-pSAR + saRNA (0.01 mg mL^{-1}). Cells were incubated for 1 and 4 hours at 37 °C with 5% CO_2. Then, nanoparticles were aspirated, and cells washed 3 times with PBS and stained with 10 μg mL^{-1} Hoechst 33342 and 75 nM Lysotracker red applied in PBS solution. After 30 minutes, solution was aspirated, and cells were washed 3 times with PBS then FluoroBrite DMEM was added to cells. Imaging was performed using Leica confocal microscopy with LAS X software on DAPI, FITC and Lysotracker filters. ImageJ software was used to process the pictures.

Imaging flow cytometry. Caco-2 cells were seeded in a clear 6-well plate at a density of 40×10^5 cells per well. For the treatment, the medium was aspirated, and cells were transfected with Opti-MEM containing BDD-pSAR + saRNA (0.01 mg mL^{-1}) formulation. After 4 hours, nanoparticles were aspirated and 150 μL of 0.05% trypsin was used for detachment of cells from wells. After incubation for 15 minutes, 300 μL FACS buffer was used to neutralise the trypsin and cells were centrifuged at 1500 rpm for 10 minutes. Following this, cells were stained with Zombie Violet (1 : 500) dye for 30 minutes at room temperature in order to help with gating on live cells. Then, cells were fixed with 100 μL of 4% paraformaldehyde in PBS for 20 minutes. Fixed cells were centrifuged, and pellets resuspended in 50 μL of PBS. Data were acquired using an Image Stream 100 (Amnis, Seattle, US) and on single cell in focus events was used for analysis. Ideas Software (Amnis, Seattle, WA, USA) was used for data analysis. Total cell fluorescence was calculated by default total cell masks for the measurement of the nanoparticle internalisation and cell interiors were identified using the area erode tool (brightfield channel). Internalisation index was shown as percentage of maximum internalisation (percentage of interior cell fluorescence to total cell fluorescence).

Isolation of tissue-derived colorectal cancer organoids. Fresh colorectal tumour tissue harvested from surgical human specimens was used to obtain patient-derived colorectal cancer organoids (ethics: 17/EM/0126). The harvested tissues were fragmented using a scalpel blade and scissors to mechanically dissociate intestinal glands. Additionally, DNase I and Liberase were added for 1 hour at 37 °C to prevent cell clumping and to increase single-cell yield. After incubation, the sample was diluted with Advanced DMEM and FBS to inactivate the enzymes and filtered using a 70 μm cell strainer to remove clumps. The filtered mixture was centrifuged, and the cell pellet was resuspended with cold Matrigel. In a pre-warmed 48 well plate, Matrigel with cells was drop casted and transferred to the incubator 10 minutes allowing the gel to form before the addition of IntestiCult™ organoid growth medium (OGM) (Stem Cell Technologies).

Colorectal patient-derived organoids culture. The culture media for colorectal patient-derived organoids was a complete cell culture medium for intestinal 3D organoids, IntestiCult™ OGM. To split organoids and dissolve Matrigel mechanical dis-

 This journal is © The Royal Society of Chemistry 2024

Open Access Article. Published on 11 abril 2024. Downloaded on 15/09/2024 5:24:48.
This article is licensed under a Creative Commons Attribution 3.0 Unported Licence.

sociation (vigorous pipetting) with cold advanced DMEM was used. The diluted sample of Matrigel with organoids was centrifuged and the organoid pellet was resuspended with TrypLE cell dissociation reagent for 10 minutes at 37 °C. After incubation, the cell suspension was diluted with advanced DMEM, centrifuged and the supernatant was discarded. Single cells and small clusters derived from fragmented organoids were encapsulated with fresh cold Matrigel and drop casted in a pre-warmed 48 well plate. After 10 minutes of incubation at 37 °C to allow the gel formation, IntestiCult™ OGM was added. The passage of colorectal patient-derived organoids in Matrigel was performed every 5–10 days.

Nanoparticles transfection in patient-derived organoids. Once colorectal patient-derived organoids had reached the desired compaction level (5 days after splitting), a formulation of 50%-pSar (w/w 128) (1.28 mg mL^{-1}) containing GFP-saRNA (10 μg mL^{-1}) was mixed with the above-mentioned organoid media, using 300 μL of the polyplex solution and 2700 μL from the organoid media. Then this solution was added onto the colorectal patient-derived organoids. After 4 hours incubation, nanoparticles were removed, and fresh media was replaced onto the organoids. GFP expression was imaged after 24 and 48 hours using a Leica confocal microscope with LAS X software and GFP filters. ImageJ software was used to process the images.

Statistical analysis

Graphs and statistics were prepared in GraphPad Prism 9.5.1 version or higher. Statistical differences were analysed using either one-way or two-way ANOVA adjusted for multiple comparison (either Tukey's or Dunnet's), p value lower than 0.05 was considered as statically significant and the levels of statistical significance were set $p^{*} < 0.05$, $p^{**} < 0.01$, $p^{***} < 0.001$ and $p^{****} < 0.0001$.

Results and discussion

Synthesis and characterisation of PBAEs

In the first step a poly(β-amino ester) was prepared from 1,4-butanediol diacrylate (BDD) and 5-aminopentanol (5AP), *via* a Michael-addition based step-growth polymerization with 10 mol% excess of BDD in relation to 5AP, to ensure termination of the polymer with acrylate groups (pBDD-5AP). After purification by precipitation in diethyl ether, acrylate end groups (6.1 ppm) were confirmed using ^{1}H NMR spectroscopy which when integrated against signals from the methylene BDD-5AP repeating unit (1.62 ppm), revealed an average DP of 15 for the pBDD-5AP PBAE (Fig. 2A and Scheme S1† and spectrum S1). SEC analysis revealed an $M_{n,SEC}$ = 6200 g mol^{-1} compared to an $M_{n,NMR}$ = 4500 g mol^{-1} and $Đ$ = 1.3. Although $Đ$ = 2 is the expected theoretical value for step-growth polymerisations at high conversion, the lower $Đ$ observed is likely due to the precipitation procedure removing low molar mass oligomers thus narrowing the molar mass distribution and increasing the average molar masses, which was indeed observed. The selection of this PBAE composition was based on prior pre-clinical investigations, which demonstrated that pBDD-5AP PBAEs can display good formulation characteristics (such as small particle size, high colloidal stability, and high zeta potentials) and potent transfection performance, both *in vitro* and *in vivo*, with various types of nucleic acid cargoes.[36]

Before producing our pSar conjugated PBAE, we first generated a sarcosine *N*-carboxyanhydride (SarNCA) from *N*-Boc-sarcosine (Boc-Sar) using a moisture-tolerant protocol developed by Lu and co-workers (Scheme S1† and Fig. 2A).[37] SarNCA was then converted into pSar-cystamine, a pSar derivative containing a single disulfide bond in the middle of the chain, using ring opening polymerisation from a bifunctional cystamine initiator targeting a DP of 18 on each side (DP = 36 in total). This relatively low DP was chosen to mimic the low molar masses used for the DMG-PEG lipid (M_n = 2000 g mol^{-1}) in the lipid nanoparticles for the commercially available SARS-CoV-2 mRNA vaccines.[38] After purification and isolation through precipitation in diethyl either, pSar-cystamine was characterised by ^{1}H NMR spectroscopy revealing an experimental DP of 20 on each side of the disulfide. This was calculated using integrals of cystamine signals at 3.70 ppm and methyl signals for the sarcosine repeating units at 2.80 ppm (Fig. 2A and spectrum S2). The higher-than-expected DP may be due to a slight initiator inefficiency or impurities within cystamine for NCA polymerisation. DMF-SEC analysis of pSar-cystamine exhibited a monomodal chromatogram with low dispersity ($Đ$ = 1.1) which as expected for NCA polymerisation. The $M_{n,SEC}$ = 3100 g mol^{-1} was close to theoretical values for DP40 pSar + cystamine ($M_{n,th}$ = 3700 g mol^{-1}) however the deviation observed is likely due to the use of PMMA standards in the SEC calibration which do not accurately represent pSar (Fig. S1†).

To conjugate pSar to the acrylate functional PBAE pBDD-5AP, first the disulphide bridge was reduced *in situ* into reactive thiols using tris(hydroxypropyl)phosphine (THP) to initiate a base catalysed thia-Michael addition reaction between the pSar chains and acrylate functional PBAE. The conjugation reaction was conducted with an excess of pSar per acrylate end-group. Following the reaction, pSar-(pBDD-5AP)-pSar was isolated and excess pSar was removed through dialysis against DMF, followed by precipitation in a diethyl ether. ^{1}H NMR spectroscopy confirmed the successful conjugation of pSar to the PBAE, generating pSar-(pBDD-5AP)-pSar (Fig. 2 and spectrum S3), revealing quantitative conversion of acryloyl groups (no visible signals at 5.9–6.4 ppm) and the expected ratio between pBDD-5AP and pSar repeating units, calculated from the pBDD-5AP methylene signals at 1.62 ppm and 2.80 ppm from methyl groups from pSar. This also confirms the removal of excess pSar that was available in the conjugation reaction. SEC analysis revealed a clear shift towards higher molar mass ($M_{n,SEC}$ = 7600 g mol^{-1}) following the reaction, indicating successful pSar conjugation.

As a control polymer without pSar, we also synthesised a hydroxyl terminated PBAE, OH-(pBDD-5AP)-OH, by endcapping the acrylate functional pBDD-5AP with further 5-AP, with

Open Access Article. Published on 11 abril 2024. Downloaded on 15/09/2024 5:24:48.
This article is licensed under a Creative Commons Attribution 3.0 Unported Licence.

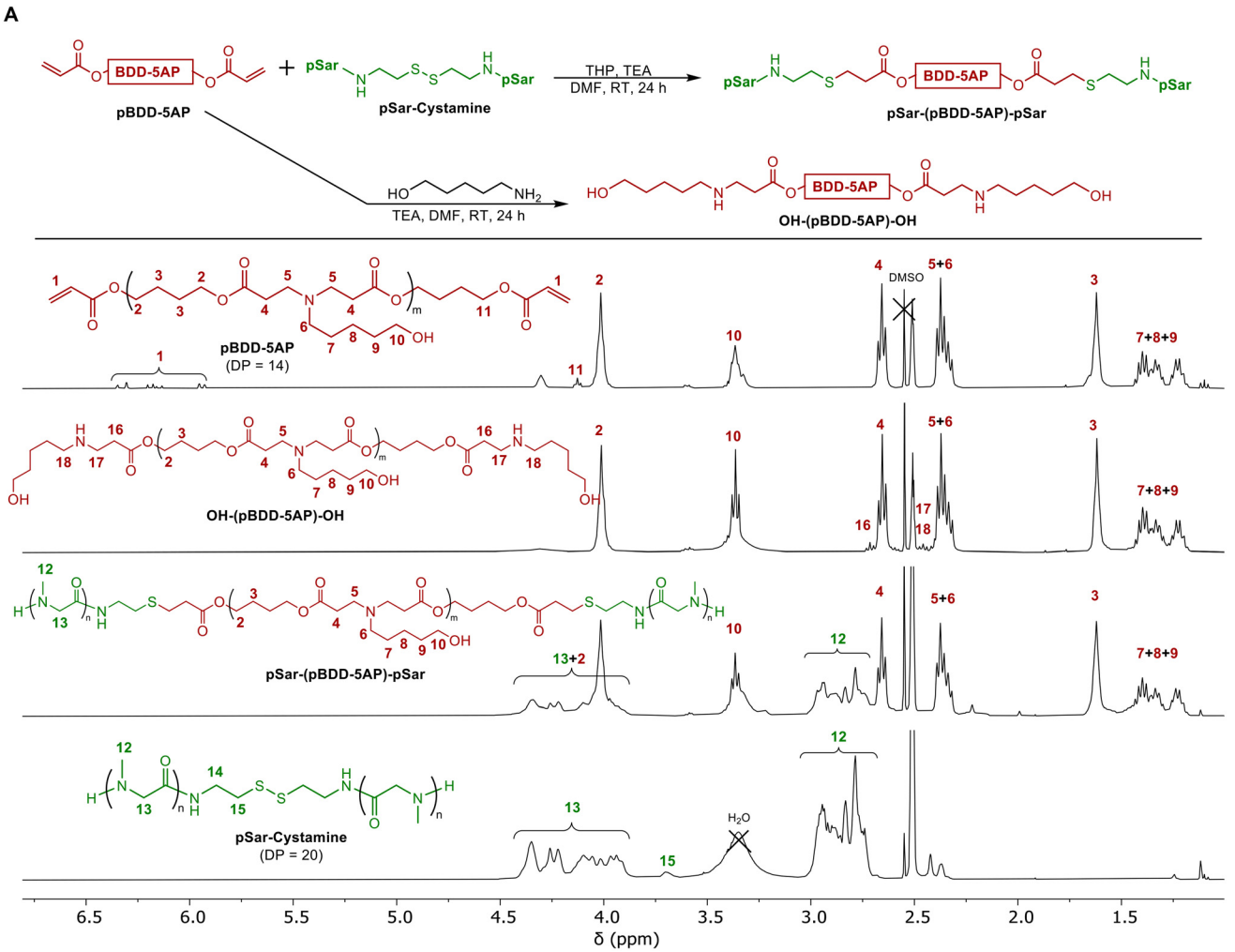

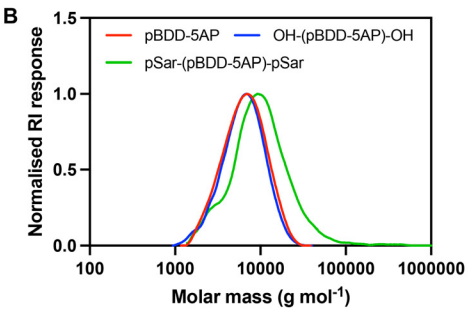

C

Polymer	$M_{n,SEC}$	$M_{w,SEC}$	$Đ$	DP pBDD-5AP	Total DP pSar
pSar-Cystamine	3100	3500	1.1	-	40
pBDD-5AP	6200	8000	1.3	15	-
OH-(pBDD-5AP)-OH	6200	13500	2.1	15	-
pSar-(pBDD-5AP)-pSar	7600	22000	2.9	15	40

Fig. 2 Synthesis and characterisation of PBAEs. (A) Synthetic scheme for step-growth Michael-addition polymerisation of BDD, 5-AP and pSar-cystamine to produce pSar-PBAE-pSar triblock copolymer. ^{1}H NMR (400 MHz, DMSO-d_6) spectra of pBDD-5AP, pSar-cystamine, and pBDD-5AP-pSar (B) GPC chromatograms of pBDD-5AP, OH-(pBDD-5AP)-OH and pSar-(pBDD-5AP)-pSar, and (C) molecular weights and dispersity values of the PBAEs produced determined using DMF-SEC, and the DP of each block of the PBAEs determined *via* ^{1}H NMR spectroscopy.

^{1}H NMR spectroscopy confirming full disappearance of acrylate end groups (Fig. 2A and spectrum S4). Size exclusion chromatographs of the synthesised polymers revealed the pre-functionalised PBAE, pBDD-5AP, exhibited $M_{n,SEC}$ of 6200 g mol^{-1} and $Đ$ = 1.3, similar to other reported PBAEs (Fig. 2B and C). Upon functionalisation with 5AP to produce OH-(pBDD-5AP)-OH, there was no significant increase in molar mass ($M_{n,SEC}$ = 6200 g mol^{-1}, and $Đ$ = 2.1). Overall, our characterisation data confirmed the successful synthesis of our targeted pSar conjugated PBAE and control polymers.

The buffering capacities were assessed for OH-(pBDD-5AP)-OH and pSar-(pBDD-5AP)-pSar as the pK_a of polycations has been recognised as crucial for enhancing endosomal buffering and endo/lysosomal escape of polymer-based nucleic acid delivery systems. Acid–base titration in the pH range of 10.0–3.0 for PBAEs with and without pSarylation displayed similar titration

This journal is © The Royal Society of Chemistry 2024

curves, implying that pSarylation did not impact their buffering capacity (Fig. S2 and Table S1†). Specifically looking at the range related to endosomal acidification, considered between pH 7.4 and pH 5.0,[39] PEI displayed a buffering capacity 12 mol of H^+ per mol of ionisable nitrogen in this pH range, whilst OH-(pBDD-5AP)-OH and pSar-(pBDD-5AP)-pSar displayed buffering capacities of 4.0 and 3.5 respectively. The weaker buffering capacities observed for the PBAEs, compared to a branched PEI control, was likely due to PEI's structure containing a high density of primary, secondary and tertiary amines compared to our PBAEs only exhibiting tertiary amines at a reduced density across the polymer chain. This therefore broadens the buffering capacity of PEI and the high density also imparts a neighbouring group effect commonly seen with ionisable polycations.

Open Access Article. Published on 11 abril 2024. Downloaded on 15/09/2024 5:24:48.
This article is licensed under a Creative Commons Attribution 3.0 Unported Licence.

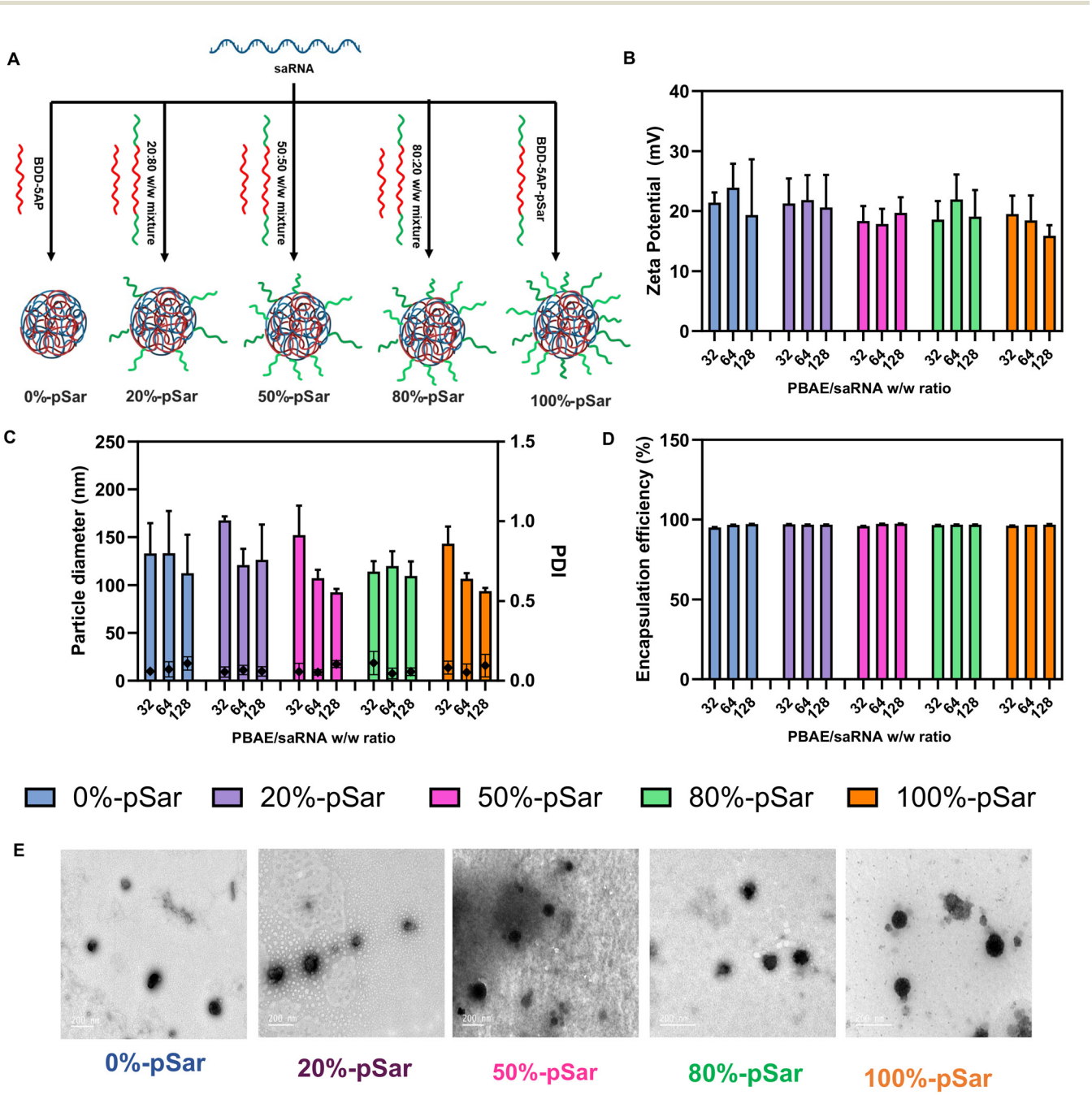

Fig. 3 Formulation of PBAEs with saRNA to produce polyplex nanoparticles. (A) Schematic representation of saRNA formulation with OH-(pBDD-5AP)-OH, pSar-(pBDD-5AP)-pSar or different mixtures, called 'mix' of pSar-(pBDD-5AP)-pSar and OH-(pBDD-5AP)-OH as a weight% which is termed as 0%-pSar, 20%-pSar, 50%-pSar, 80%-pSar and 100%-pSar. The nanoparticles were prepared in pH 5.0 25 mM sodium acetate at a final saRNA concentration of 10 μg mL^{-1}. (B) Zeta potential and (C) particle size for the OH-(pBDD-5AP)-OH, pSar-(pBDD-5AP)-pSar and 'mix' polyplexes at a PBAE/saRNA w/w ratio of 32, 64 and 128 determined by dynamic light scattering at 25 °C. Bars represent the mean ± SD. (D) Encapsulation efficiency of saRNA within polyplexes evaluated using Ribogreen assay. (E) Representative transmission electron micrograph of all polyplexes.

Open Access Article. Published on 11 abril 2024. Downloaded on 15/09/2024 5:24:48.
This article is licensed under a Creative Commons Attribution 3.0 Unported Licence.

Effect of pSar density on polyplex physicochemical properties

Polyplex preparation was performed at three different polymer/fluc saRNA weight-to-weight ratios (w/w ratios of 32, 64 and 128) for OH-(pBDD-5AP)-OH and pSar-(pBDD-5AP)-pSar PBAEs to optimise the physicochemical properties of the polyplex. These include particle size, surface charge, encapsulation efficiency, biocompatibility, and RNA expression. To assess the effect of pSar density on the nanoparticle surface, we also prepared polyplexes prepared with 20%-pSar, 50%-pSar and 80%-pSar which are mixtures of pSar-(pBDD-5AP)-pSar and OH-(pBDD-5AP)-OH as a weight% (Fig. 3A). Briefly polyplexes were prepared by mixing the desired polymers and saRNA in pH 5.0 sodium acetate buffer. Varying quantities of polymer stock solutions, depending on the desired w/w ratio, were then combined with saRNA manually using a micropipette and allowed to incubate at ambient temperature for 30 minutes. It should also be noted that in the literature there are different approaches to modulate the ratio of nucleic acid cargo to the polymer delivery vector. One common approach is a simple weight ratio between the nucleic acid and polymer, which is more common in the PBAE literature for pharmaceutical development. However, many researchers also consider the nitrogen to phosphate ratio (N/P) as a way to identify a charge ratio and normalise for different materials. In this study we opted for weight to weight ratios to be consistent with previous literature on PBAEs and polymer-conjugated PBAEs,[40] however we have also reported the N/P ratios for comparison with other literature (Table S2†).

Hydrodynamic diameters of all nanoparticles were observed to be between 100–150 nm with low polydispersity index (PDI) values (<0.2), regardless of pSar content, determined by dynamic light scattering (DLS) (Fig. 3C). Some particles *e.g.* 50%-pSar and 100%-pSar possessed a significantly decreasing size with w/w ratio. In addition, zeta potential of the particles was measured to be between 20–25 mV and no significant difference was observed between the groups (Fig. 3B). The

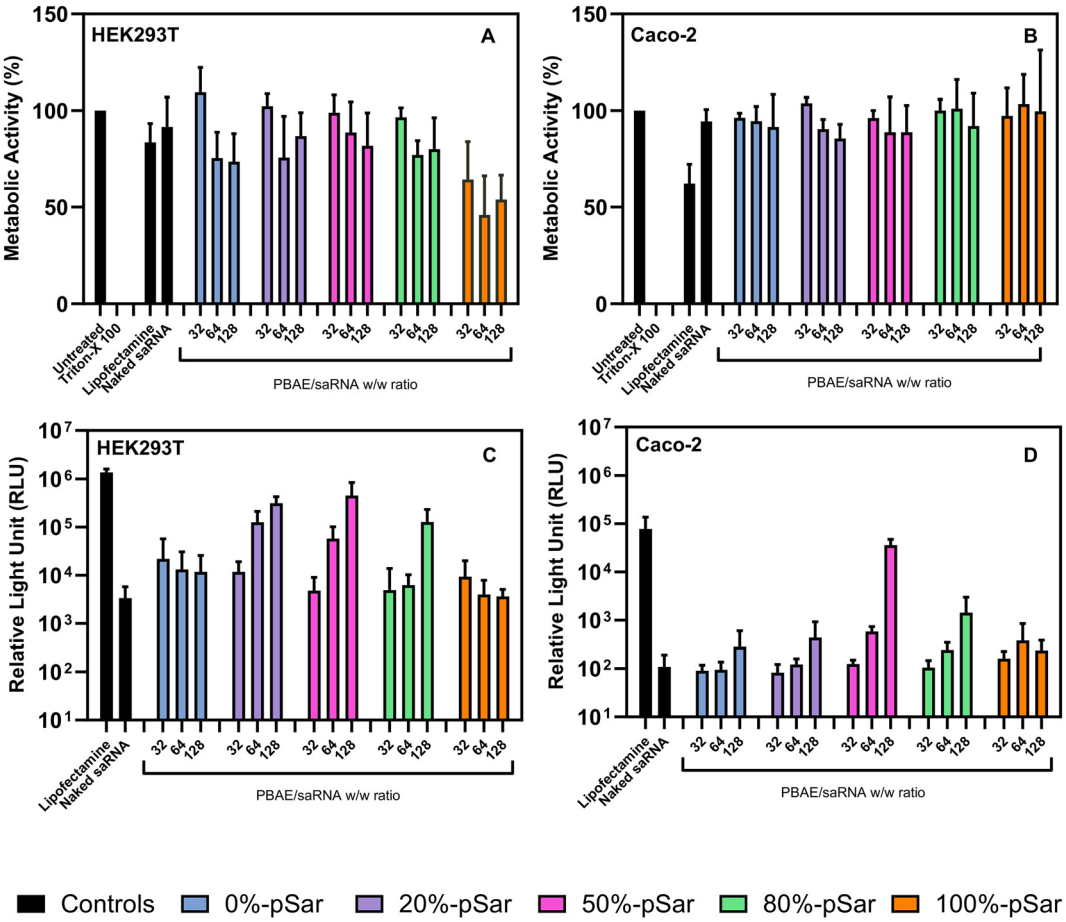

Fig. 4 Metabolic activity and transfection efficiency of PBAE derived saRNA polyplexes. Effect of PBAE polyplexes formulated with firefly luciferase encoding saRNA at PBAE/saRNA w/w ratios of 32, 64 and 128 on metabolic activity (A and B) and transfection efficiency (C and D) on HEK293T cells (A and C) and Caco-2 cells (B and D). Cells were treated with polyplexes containing saRNA at a concentration of 500 ng mL^{-1} (100 ng per well) in serum-free Opti-MEM. Metabolic activity was compared against Triton X (positive control) and untreated cells (negative control), and calculated by normalizing metabolic activity to untreated cells. *In vitro* transfection efficiency was analysed after 24 h post-transfection using the Promega ONE-GLO luciferase assay and compared against Lipofectamine Messenger MAX™ (positive control) and naked saRNA (negative control) expressed as relative light units (RLU) for luciferase expression. Bars represent the mean ± SD.

This journal is © The Royal Society of Chemistry 2024

Open Access Article. Published on 11 abril 2024. Downloaded on 15/09/2024 5:24:48.
This article is licensed under a Creative Commons Attribution 3.0 Unported Licence.

encapsulation efficiency of nanoparticles was analysed utilizing Ribogreen assay and revealed full RNA encapsulation for nanoparticles produced at all pSar-(pBDD-5AP)-pSar/OH-(pBDD-5AP)-OH ratios (Fig. 3D). Finally, TEM micrographs of all polyplexes prepared at a w/w ratio of 128 displayed spherical complexes between 35 to 220 nm in diameter consistent with DLS analysis and taking into account some particle shrinking in the dry state (Fig. 3E). Furthermore, as DLS analysis can over represent larger particles present in heterogeneous particle distributions, it is likely that any smaller species visible by TEM may not have been included in the particle size averages.[41] Overall, these results indicate that all five formulations were capable of encapsulating saRNA and producing particle sizes below the typical 200 nm diameter threshold for efficient gene delivery.

In vitro evaluation of saRNA delivery

Transfection and metabolic activity of pSarylated polyplexes. The toxicity and saRNA delivery/expression efficiency of the individual OH-(pBDD-5AP)-OH, pSar-(pBDD-5AP)-pSar and co-formulated polyplexes were examined in HEK293T and Caco-2 cell lines. These cell lines were chosen as HEK23T human kidney cell line is the main cell line used for pilot transfection studies as are they are easy to transfect, and culture, whilst Caco-2 colon cancer cell line is a model of intestinal barrier integrity and can spontaneously differentiate into a heterogenous mixture of intestinal epithelial cells as occurs in the intestine. Similar to the formulation characterisation study above, polyplexes were prepared at polymer/saRNA w/w ratios of 32, 64, and 128, utilising a firefly luciferase encoding saRNA and compared against Lipofectamine MessengerMAX™ (positive expression control) and Triton X-100 (positive toxicity control). All the formulations exhibited more than 50% cell viability, as determined from the metabolic activities. Similar to previous studies, increasing w/w ratio, specifically above w/w 32, resulted in increased toxicity due to increased polycation concentration which is known to disrupt the negative phospholipid bilayer[42] (Fig. 4A). In general, Caco-2 cells displayed high metabolic activity compared to HEK293T cells which may be due to the lower transfectability of the intestinal epithelial cells (Fig. 4B).[43] Notably, using HEK293T cells, formulations prepared at higher w/w ratios yielded greater trans-

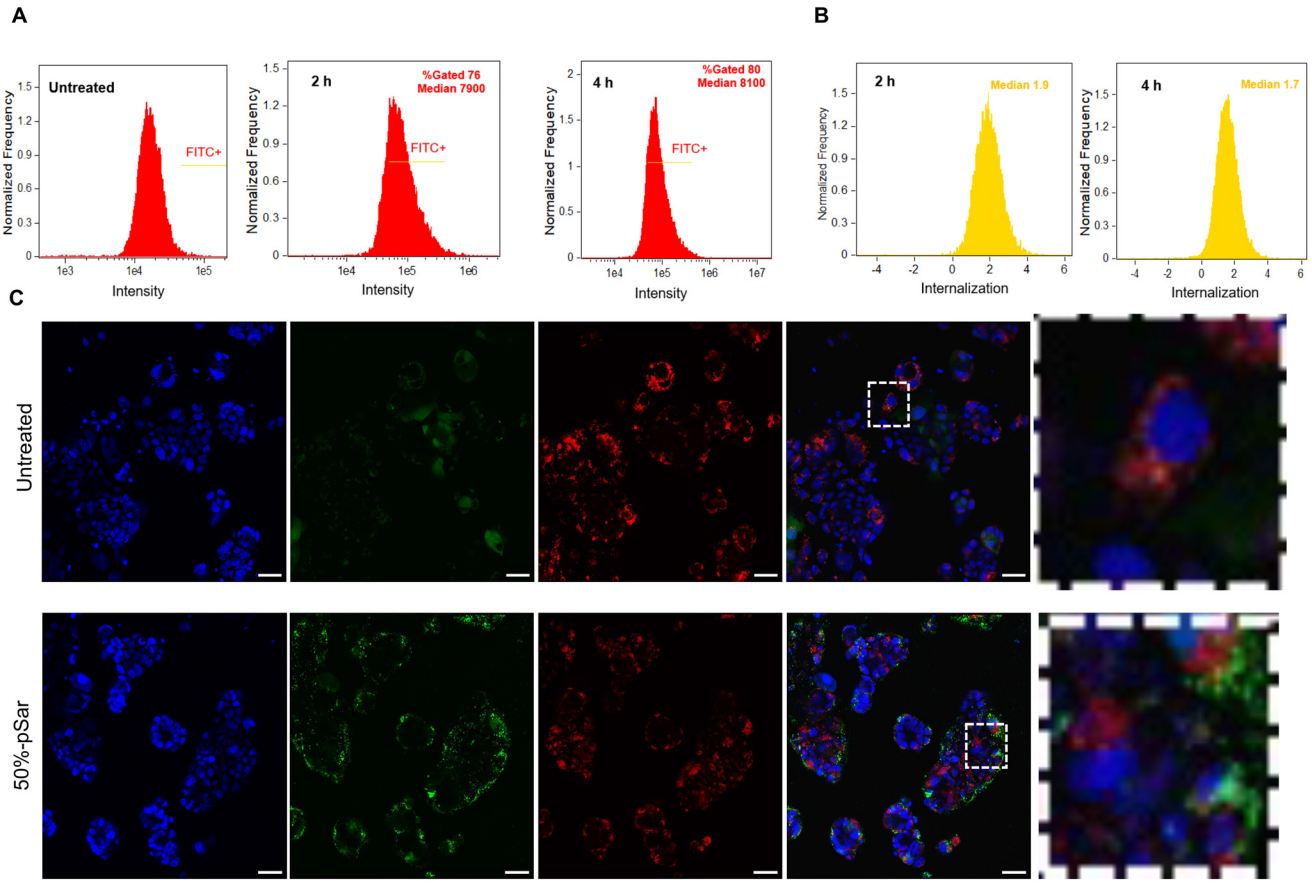

Fig. 5 Cellular uptake of PBAE derived saRNA polyplexes. (A and B) Imaging cytometry histograms of fluorescence intensity and internalisation for Caco-2 cells after 2 h and 4 h following treatment with FITC-labelled 50%-pSar polyplexes at a PBAE/saRNA w/w ratio of 128 at a concentration of 500 ng mL^{-1} saRNA. Data were analysed using IDEAS software. (C) Representative confocal microscopy images of Caco-2 cells treated saRNA polyplexes derived from FITC-labelled pSar-(pBDD-5AP)-pSar at a PBAE/saRNA w/w ratio of 128 for 50%-pSar polyplexes after 4 h at 100 ng per well (500 ng mL^{-1}) saRNA. Scale bar 10 μm (63×).

Open Access Article. Published on 11 abril 2024. Downloaded on 15/09/2024 5:24:48.
This article is licensed under a Creative Commons Attribution 3.0 Unported Licence.

fection efficacy explicitly for co-formulated groups (20%-pSar, 50%-pSar and 80%-pSar) (Fig. 4B). For the w/w ratio 128 the transfection efficiency was close in extent to the positive control, Lipofectamine MessengerMAX™. Unlike in HEK293T cells most of the formulations did not show statistically significantly higher luciferase expression than naked saRNA in Caco-2 cells; however, only the polyplexes 50%-pSar and 80%-pSar yielded increased saRNA expression in this cell line. Particularly, no substantial difference was detected between the 50%-pSar and positive control lipofectamine. Similarly, a previous study showed that mixed of PEGylated and non-PEGylated polymers (50 : 50) displayed the most effective gene delivery vector for glioblastoma cells.[40]

Cellular uptake of pSarylated polyplexes. Due to the encouraging results with 50%-pSar polyplex at w/w 128, we further investigated cellular uptake of this polyplex formulation. To evaluate the cellular association of 50%-pSar polyplexes in Caco-2 cells, we first generated a FITC labelled pSar-(pBDD-5AP)-pSar through alcohol isothiocyanate coupling on the pendant hydroxyl groups of the 5-AP monomers within the core PBAE. Cellular uptake was assessed through imaging flow cytometry 2 h and 4 h after treatment (Fig. 5A). It was observed that 76% of Caco-2 cells were FITC-positive, indicating successful cell association within 2 hours of incubation. There was a further increase to 80% FITC-positive at 4 h incubation time, overall highlighting rapid association of the administered polyplexes. The median fluorescence intensity rose from 7900 arbitrary units up to 8100 between 2 h and 4 h incubation, indicating an initial rapid uptake by the Caco-2 cells and release into the cytosol occurred within 2 hours in this experiment. Compared to traditional flow cytometry the images from each cell can be analysed to compare internalisation *vs.* membrane association. The median of internalisation score of the polyplexes was approximately 1.8 indicating a high proportion of nanoparticles were internalised inside the cells since having a score less than 0.3 can be considered to be surface bound (Fig. 5B).[44]

To assess further the intracellular internalisation mechanism of the pSar-(pBDD-5AP)-pSar in Caco-2 cells we employed confocal microscopy to evaluate colocalization with a lysosomal (Lysotracker™ red) and nuclear (Hoecht 33342) stain (Fig. 5C). After 4 h post administration, confocal micrographs showed that polyplexes successfully internalised within Caco-2 and merged images demonstrated with minimal co-localisation with the acidic lysosomes with image analysis indicating Pearson's correlation coefficient between FITC labelled polyplexes and Lysotracker™ stained lysosomes were below 0.5. Given the ~100 nm particle diameters it is likely that these formulations were internalised by an endocytosis mechanism, however the apparent low colocalization with the acidic lysosomes may indicate that the particles escaped before endosomal maturation to lysosomal compartments. Although further endosomal escape studies would be needed to investigate this phenomenon in more detail, it is possible that enhanced endosomal escape was a factor in the high expression efficiencies observed for these complexes. However,

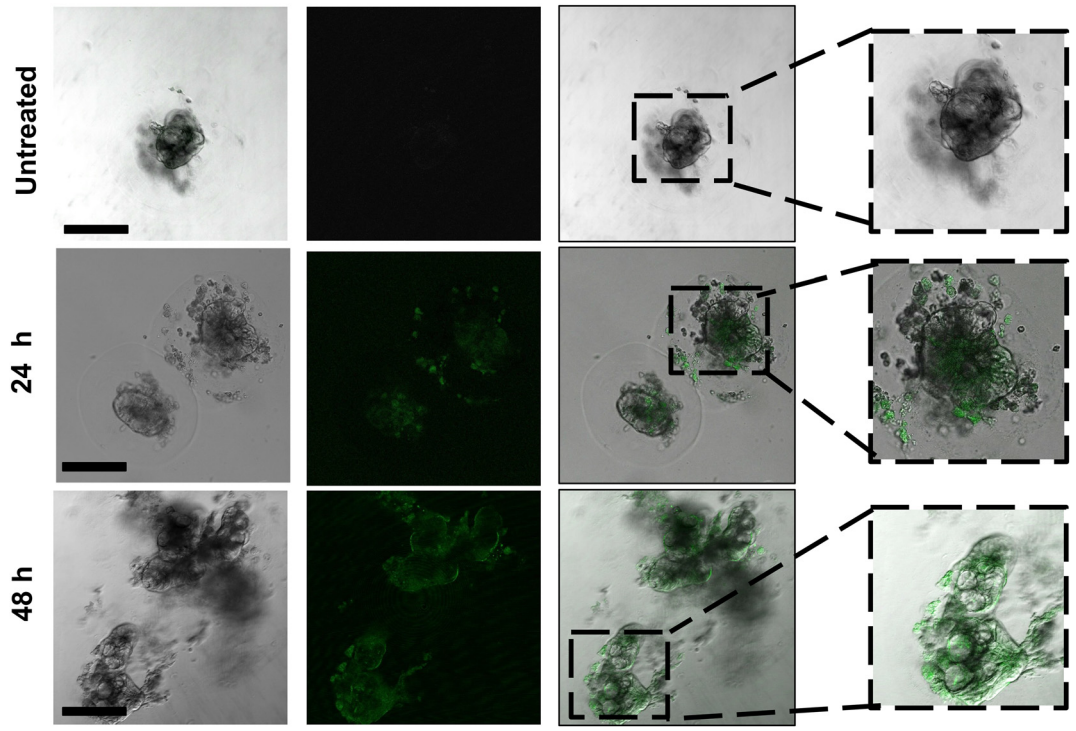

Fig. 6 Penetration and saRNA expression of PBAE polyplexes in colorectal cancer organoids. Analysis of GFP expression of 50%-pSar in human colon colorectal cancer organoids using confocal microscopy after 24 and 48 h (40× – scale bar 100 μm).

 This journal is © The Royal Society of Chemistry 2024

Open Access Article. Published on 11 abril 2024. Downloaded on 15/09/2024 5:24:48.
This article is licensed under a Creative Commons Attribution 3.0 Unported Licence.

it should also be noted that fluorescein is a pH responsive dye hence may exhibit reduced fluorescence within the acidic lysosomal compartments, adding an uncertainty to measures of dye co-localisation, nonetheless the high transfection efficiencies observed for this formulation indicates clear propensity of endosomal escape which may have all escaped within the first 2 hours.

Assessment of pSarylated polyplexes in colorectal cancer organoids. Following successful *in vitro* saRNA transfection and polyplex uptake of 50%-pSar (w/w 128) in Caco-2 cells, we hypothesised that this material may be an effective in delivering saRNA to intestinal organoids. Organoids are 3D organ-like structures that are cultivated from human tissue-derived stem cells in a laboratory setting. For instance, colon organoids comprise stem cells, goblet cells, enterocytes, endocrine cells, paneth cells and transit amplifying cells. These organoids naturally form complex structures, mimicking some aspects of real organ physiology, which holds promise for translating preclinical research into clinical applications.[45]

We therefore evaluated our chosen formulation 50%-pSar (w/w 128) encapsulating a GFP-saRNA in human colon colorectal organoids to monitor saRNA expression *via* confocal microscopy. The 50%-pSar saRNA formulation was incubated with organoids once they had reached the desired compaction level. After 4 h, nanoparticles were removed, and fresh media was replaced onto the organoids. GFP expression was determined after 24 and 48 h. Confocal microscopy revealed GFP expression within the central regions of the organoids at 24 h, with increasing fluorescence intensity observable after 48 h (Fig. 6). Previous studies have shown expression of exogenously delivered nucleic acids at the surface of cancer organoids, however the 50%-pSar PBAE formulations were substantially improved compared to the prior systems in terms of generating high expression levels deep within the core of the organoid, indicating high penetration of these nanoparticles within the dense matrix of cells.[46,47] These results indicate that pSarylated PBAEs may represent promising new materials for tumour directed delivery of nucleic acid therapeutics. Additionally, the full preservation of the organoid structure over the 48 h transfection experiment may suggest that these materials could be used to aid delivery of mRNA and saRNA to further organoid models to examine how expression of exogenously administered RNA varies within the surface and core of these tumour models.

Conclusions

In this work we have developed a new methodology to produce polysarcosinylated poly(beta amino esters) as an alternative steric stabilising group to PEG. We used this new pSar-PBAE conjugate to produce a library of polyplexes with different pSar densities on the nanoparticle surface by mixing pSarylated PBAEs with analogous unfunctionalized PBAEs in different ratios. We observed that pSarylation had minimal effect on polyplex physicochemical properties, while all pSar densities yielded higher transfection efficiencies than the positive control lipofectamine in HEK293T cells. In contrast, only the 50%-pSar polyplexes produced saRNA expression comparable to lipofectamine in colorectal cancer cells (Caco-2), with uptake studies indicating fast cellular uptake and limited co-localization in lysosomes indicating potential for endosomal escape. Finally, the 50%-pSar polyplexes showed potential translation for tumour delivery, exhibiting high expression of saRNA within the core colorectal cancer organoids within 24 h, likely due to the enhanced permeability of these polyplexes endowed with the pSar coating. The efficient diffusion to the organoid core may make these formulations amenable to intratumoural delivery of genetic material encoding for pro-inflammatory cytokines which are required for stimulation of the immune system around the local tumour environment in immuno-oncology applications. Overall, these results indicate that pSarylation is a suitable alternative for PEGylation of PBAEs, yielding potent gene delivery vehicles. As pSar is an established PEG alternative, future research should focus on studying the differences in immunogenicity between PEG-PBAE and pSar-PBAE conjugates, which is especially important for vaccine and immunotherapy nucleic acid formulations.

Data access statement

All relevant data can be obtained upon request from the corresponding author at p.gurnani@ucl.ac.uk.

Author contributions

Conceptualization, H. B. and P. G.; data curation and formal analysis, H. B., R. K. J., P. G.; writing original draft preparation, H. B.; writing review and editing, H. B., R. K. J., A. E., M. M., N. G., U. C. O., K. P., P. F. M., R. J. S., P. O. M., A. M., C. A., P. G.; supervision, A. M., C. A., P. G.; project administration, C. A., P. G.; funding acquisition, C. A. All authors have read and agreed to the published version of the manuscript.

Conflicts of interest

All authors declare that they have no conflicts of interest.

Acknowledgements

We thank the Royal Society [Wolfson research merit award WM150086 to CA]. Work on this project is supported by Wellcome Leap as part of the R3 Program [Biofoundry-in-a-Box], the Turkish Ministry of National Education, and an Engineering and Physical Sciences Research Council ICASE 2021 Studentship. Umut Can Oz is thankful for a fellowship (2219) from the TUBITAK. We also thank Tom Hyde, Esme Ireson and Paul Cooling for expert technical support. The

Nanoscale & Macroscale Research Centre (NMRC) is acknowledged for providing the facilities for TEM and related analysis particularly to Denise McLean. We thank the School of Life Sciences imaging facility (SLIM) and their staff, particularly Dr Tim Self, for use of their facilities and expert guidance. We thank the MINIGUTS team (consultants, pathologists, scientists and nurses) for recruiting patients, and helping with the collection of colon cancer patients' biopsies at Queen's Medical Centre (QMC), Nottingham.

Open Access Article. Published on 11 abril 2024. Downloaded on 15/09/2024 5:24:48.
This article is licensed under a Creative Commons Attribution 3.0 Unported Licence.

References

1 Y. Zhong, S. Du and Y. Dong, mRNA delivery in cancer immunotherapy, *Acta Pharm. Sin. B*, 2023, **13**(4), 1348–1357.
2 N. Pardi, M. J. Hogan, F. W. Porter and D. Weissman, mRNA vaccines - a new era in vaccinology, *Nat. Rev. Drug Discovery*, 2018, **17**(4), 261–279.
3 D. Li, C. Liu, Y. Li, R. Tenchov, J. M. Sasso, D. Zhang, D. Li, L. Zou, X. Wang and Q. Zhou, Messenger RNA-Based Therapeutics and Vaccines: What's beyond COVID-19?, *ACS Pharmacol. Transl. Sci.*, 2023, **6**(7), 943–969.
4 B. Fayed, J. Jagal, R. Cagliani, R. A. Kedia, A. Elsherbeny, H. Bayraktutan, G. Khoder and M. Haider, Co-administration of amoxicillin-loaded chitosan nanoparticles and inulin: A novel strategy for mitigating antibiotic resistance and preserving microbiota balance in Helicobacter pylori treatment, *Int. J. Biol. Macromol.*, 2023, **253**, 126706.
5 Z. A. Azrak, M. S. Taha, J. Jagal, A. Elsherbeny, H. Bayraktutan, M. H. AbouGhaly, A. H. Elshafeey, K. Greish and M. Haider, Optimized mucoadhesive niosomal carriers for intranasal delivery of carvedilol: A quality by design approach, *Int. J. Pharm.*, 2024, 123935.
6 A. K. Blakney, Y. Zhu, P. F. McKay, C. R. Bouton, J. Yeow, J. Tang, K. Hu, K. Samnuan, C. L. Grigsby, R. J. Shattock and M. M. Stevens, Big Is Beautiful: Enhanced saRNA Delivery and Immunogenicity by a Higher Molecular Weight, Bioreducible, Cationic Polymer, *ACS Nano*, 2020, **14**(5), 5711–5727.
7 S. Taranejoo, J. Liu, P. Verma and K. Hourigan, A review of the developments of characteristics of PEI derivatives for gene delivery applications, *J. Appl. Polym. Sci.*, 2015, **132**(25), 42096.
8 A. K. Blakney, P. F. McKay, K. Hu, K. Samnuan, N. Jain, A. Brown, A. Thomas, P. Rogers, K. Polra, H. Sallah, J. Yeow, Y. Zhu, M. M. Stevens, A. Geall and R. J. Shattock, Polymeric and lipid nanoparticles for delivery of self-amplifying RNA vaccines, *J. Controlled Release*, 2021, **338**, 201–210.
9 P. Gurnani, A. K. Blakney, J. Yeow, C. R. Bouton, R. J. Shattock, M. M. Stevens and C. Alexander, An improved synthesis of poly(amidoamine)s for complexation with self-amplifying RNA and effective transfection, *Polym. Chem.*, 2020, **11**(36), 5861–5869.
10 H. Bayraktutan, P. Symonds, V. Brentville, A. Mata, L. Durrant, C. Alexander and P. Gurnani, Sparsely Pegylated Poly (Beta-Amino Esters) Polyplexes Enhance Antigen Specific T-Cell Response of a Bivalent Sars-Cov-2 DNA Vaccine. Available at SSRN 4695805.
11 X. Wang, Z. Zhang and N. Hadjichristidis, Poly(amino ester)s as an emerging synthetic biodegradable polymer platform: Recent developments and future trends, *Prog. Polym. Sci.*, 2023, **136**, 101634.
12 N. K. Dastgerdi, N. Gumus, H. Bayraktutan, D. Jackson, K. Polra, P. F. McKay, F. Atyabi, R. Dinarvand, R. J. Shattock and L. Martinez-Pomares, Charge neutralized poly (β-amino ester) polyplex nanoparticles for delivery of self-amplifying RNA, *Nanoscale Adv.*, 2024, **6**, 1409–1422.
13 Y. Rui, D. R. Wilson, S. Y. Tzeng, H. M. Yamagata, D. Sudhakar, M. Conge, C. A. Berlinicke, D. J. Zack, A. Tuesca and J. J. Green, High-throughput and high-content bioassay enables tuning of polyester nanoparticles for cellular uptake, endosomal escape, and systemic in vivo delivery of mRNA, *Sci. Adv.*, 2022, **8**(1), eabk2855.
14 A. Akinc, D. M. Lynn, D. G. Anderson and R. Langer, Parallel synthesis and biophysical characterization of a degradable polymer library for gene delivery, *J. Am. Chem. Soc.*, 2003, **125**(18), 5316–5323.
15 J. S. Suk, Q. Xu, N. Kim, J. Hanes and L. M. Ensign, PEGylation as a strategy for improving nanoparticle-based drug and gene delivery, *Adv. Drug Delivery Rev.*, 2016, **99**(Pt A), 28–51.
16 Y. Liu, Y. Li, D. Keskin and L. Shi, Poly(beta-Amino Esters): Synthesis, Formulations, and Their Biomedical Applications, *Adv. Healthcare Mater.*, 2019, **8**(2), e1801359.
17 J. Kim, S. K. Mondal, S. Y. Tzeng, Y. Rui, R. Al-Kharboosh, K. K. Kozielski, A. G. Bhargav, C. A. Garcia, A. Quinones-Hinojosa and J. J. Green, Poly(ethylene glycol)-Poly(beta-amino ester)-Based Nanoparticles for Suicide Gene Therapy Enhance Brain Penetration and Extend Survival in a Preclinical Human Glioblastoma Orthotopic Xenograft Model, *ACS Biomater. Sci. Eng.*, 2020, **6**(5), 2943–2955.
18 J. H. Brumbach, C. Lin, J. Yockman, W. J. Kim, K. S. Blevins, J. F. Engbersen, J. Feijen and S. W. Kim, Mixtures of poly(triethylenetetramine/cystamine bisacrylamide) and poly(triethylenetetramine/cystamine bisacrylamide)-g-poly(ethylene glycol) for improved gene delivery, *Bioconjugate Chem.*, 2010, **21**(10), 1753–1761.
19 C. Zhu, M. Zheng, F. Meng, F. M. Mickler, N. Ruthardt, X. Zhu and Z. Zhong, Reversibly shielded DNA polyplexes based on bioreducible PDMAEMA-SS-PEG-SS-PDMAEMA triblock copolymers mediate markedly enhanced nonviral gene transfection, *Biomacromolecules*, 2012, **13**(3), 769–778.
20 C. Wang, X. Wang, L. Du, Y. Dong, B. Hu, J. Zhou, Y. Shi, S. Bai, Y. Huang, H. Cao, Z. Liang and A. Dong, Harnessing pH-Sensitive Polycation Vehicles for the Efficient siRNA Delivery, *ACS Appl. Mater. Interfaces*, 2021, **13**(2), 2218–2229.
21 G. T. Kozma, T. Shimizu, T. Ishida and J. Szebeni, Anti-PEG antibodies: Properties, formation, testing and role in

 This journal is © The Royal Society of Chemistry 2024

Open Access Article. Published on 11 abril 2024. Downloaded on 15/09/2024 5:24:48.
This article is licensed under a Creative Commons Attribution 3.0 Unported Licence.

adverse immune reactions to PEGylated nano-biopharmaceuticals, *Adv. Drug Delivery Rev.*, 2020, **154–155**, 163–175.

22 Y. Ju, W. S. Lee, E. H. Pilkington, H. G. Kelly, S. Li, K. J. Selva, K. M. Wragg, K. Subbarao, T. H. O. Nguyen, L. C. Rowntree, L. F. Allen, K. Bond, D. A. Williamson, N. P. Truong, M. Plebanski, K. Kedzierska, S. Mahanty, A. W. Chung, F. Caruso, A. K. Wheatley, J. A. Juno and S. J. Kent, Anti-PEG Antibodies Boosted in Humans by SARS-CoV-2 Lipid Nanoparticle mRNA Vaccine, *ACS Nano*, 2022, **16**(8), 11769–11780.

23 M. Barz, R. Luxenhofer, R. Zentel and M. J. Vicent, Overcoming the PEG-addiction: well-defined alternatives to PEG, from structure–property relationships to better defined therapeutics, *Polym. Chem.*, 2011, **2**(9), 1900–1918.

24 Y. W. Kong and E. C. Dreaden, PEG: Will It Come Back to You? Polyethelyne Glycol Immunogenicity, COVID Vaccines, and the Case for New PEG Derivatives and Alternatives, *Front. Bioeng. Biotechnol.*, 2022, **10**, 879988.

25 A. Elsherbeny, H. Bayraktutan, U. C. Oz, C. Moloney, J. C. Ashworth, A. M. Grabowska and C. Alexander, Responsive Nanomaterial Delivery Systems for Pancreatic Cancer Management, *Adv. Ther.*, 2023, 2300330.

26 M. Berger, F. Toussaint, S. B. Djemaa, J. Laloy, H. Pendeville, B. Evrard, C. Jerome, A. Lechanteur, D. Mottet, A. Debuigne and G. Piel, Poly(vinyl pyrrolidone) derivatives as PEG alternatives for stealth, non-toxic and less immunogenic siRNA-containing lipoplex delivery, *J. Controlled Release*, 2023, **361**, 87–101.

27 C. Pelosi, M. R. Tinè and F. R. Wurm, Main-chain water-soluble polyphosphoesters: Multi-functional polymers as degradable PEG-alternatives for biomedical applications, *Eur. Polym. J.*, 2020, **141**, 110079.

28 M. Tully, M. Dimde, C. Weise, P. Pouyan, K. Licha, M. Schirner and R. Haag, Polyglycerol for Half-Life Extension of Proteins-Alternative to PEGylation?, *Biomacromolecules*, 2021, **22**(4), 1406–1416.

29 P. Zhang, P. Jain, C. Tsao, Z. Yuan, W. Li, B. Li, K. Wu, H. C. Hung, X. Lin and S. Jiang, Polypeptides with High Zwitterion Density for Safe and Effective Therapeutics, *Angew. Chem., Int. Ed.*, 2018, **57**(26), 7743–7747.

30 A. Mero, G. Pasut, L. Dalla Via, M. W. Fijten, U. S. Schubert, R. Hoogenboom and F. M. Veronese, Synthesis and characterization of poly(2-ethyl 2-oxazoline)-conjugates with proteins and drugs: suitable alternatives to PEG-conjugates?, *J. Controlled Release*, 2008, **125**(2), 87–95.

31 A. Birke, J. Ling and M. Barz, Polysarcosine-containing copolymers: Synthesis, characterization, self-assembly, and applications, *Prog. Polym. Sci.*, 2018, **81**, 163–208.

32 S. S. Nogueira, A. Schlegel, K. Maxeiner, B. Weber, M. Barz, M. A. Schroer, C. E. Blanchet, D. I. Svergun, S. Ramishetti, D. Peer, P. Langguth, U. Sahin and H. Haas, Polysarcosine-Functionalized Lipid Nanoparticles for Therapeutic mRNA Delivery, *ACS Appl. Nano Mater.*, 2020, **3**(11), 10634–10645.

33 A. J. Geall, A. Verma, G. R. Otten, C. A. Shaw, A. Hekele, K. Banerjee, Y. Cu, C. W. Beard, L. A. Brito, T. Krucker, D. T. O'Hagan, M. Singh, P. W. Mason, N. M. Valiante, P. R. Dormitzer, S. W. Barnett, R. Rappuoli, J. B. Ulmer and C. W. Mandl, Nonviral delivery of self-amplifying RNA vaccines, *Proc. Natl. Acad. Sci. U. S. A.*, 2012, **109**(36), 14604–14609.

34 P. Gurnani, A. K. Blakney, R. Terracciano, J. E. Petch, A. J. Blok, C. R. Bouton, P. F. McKay, R. J. Shattock and C. Alexander, The In Vitro, Ex Vivo, and In Vivo Effect of Polymer Hydrophobicity on Charge-Reversible Vectors for Self-Amplifying RNA, *Biomacromolecules*, 2020, **21**(8), 3242–3253.

35 F. Saviano, T. Lovato, A. Russo, G. Russo, C. R. Bouton, R. J. Shattock, C. Alexander, F. Quaglia, A. K. Blakney, P. Gurnani and C. Conte, Ornithine-derived oligomers and dendrimers for in vitro delivery of DNA and ex vivo transfection of skin cells via saRNA, *J. Mater. Chem. B*, 2020, **8**(22), 4940–4949.

36 R. A. Cordeiro, A. Serra, J. F. Coelho and H. Faneca, Poly (β-amino ester)-based gene delivery systems: From discovery to therapeutic applications, *J. Controlled Release*, 2019, **310**, 155–187.

37 Z. Y. Tian, Z. Zhang, S. Wang and H. Lu, A moisture-tolerant route to unprotected alpha/beta-amino acid N-carboxyanhydrides and facile synthesis of hyperbranched polypeptides, *Nat. Commun.*, 2021, **12**(1), 5810.

38 C. Hald Albertsen, J. A. Kulkarni, D. Witzigmann, M. Lind, K. Petersson and J. B. Simonsen, The role of lipid components in lipid nanoparticles for vaccines and gene therapy, *Adv. Drug Delivery Rev.*, 2022, **188**, 114416.

39 A. Alazzo, N. Gumus, P. Gurnani, S. Stolnik, R. Rahman, K. Spriggs and C. Alexander, Investigating histidinylated highly branched poly(lysine) for siRNA delivery, *J. Mater. Chem. B*, 2022, **10**(2), 236–246.

40 J. Kim, S. K. Mondal, S. Y. Tzeng, Y. Rui, R. Al-kharboosh, K. K. Kozielski, A. G. Bhargav, C. A. Garcia, A. Quiñones-Hinojosa and J. J. Green, Poly(ethylene glycol)–Poly(beta-amino ester)-Based Nanoparticles for Suicide Gene Therapy Enhance Brain Penetration and Extend Survival in a Preclinical Human Glioblastoma Orthotopic Xenograft Model, *ACS Biomater. Sci. Eng.*, 2020, **6**(5), 2943–2955.

41 S. K. Filippov, R. Khusnutdinov, A. Murmiliuk, W. Inam, L. Y. Zakharova, H. Zhang and V. V. Khutoryanskiy, Dynamic light scattering and transmission electron microscopy in drug delivery: a roadmap for correct characterization of nanoparticles and interpretation of results, *Mater. Horiz.*, 2023, **10**(12), 5354–5370.

42 C. H. Jones, M. Chen, A. Ravikrishnan, R. Reddinger, G. Zhang, A. P. Hakansson and B. A. Pfeifer, Mannosylated poly (beta-amino esters) for targeted antigen presenting cell immune modulation, *Biomaterials*, 2015, **37**, 333–344.

43 V. Hiebl, D. Schachner, A. Ladurner, E. H. Heiss, H. Stangl and V. M. Dirsch, Caco-2 cells for measuring intestinal cholesterol transport-possibilities and limitations, *Biol. Proced. Online*, 2020, **22**(1), 1–18.

44 Y. Phanse, A. E. Ramer-Tait, S. L. Friend, B. Carrillo-Conde, P. Lueth, C. J. Oster, G. J. Phillips, B. Narasimhan, M. J. Wannemuehler and B. H. Bellaire, Analyzing cellular

Open Access Article. Published on 11 abril 2024. Downloaded on 15/09/2024 5:24:48.
This article is licensed under a Creative Commons Attribution 3.0 Unported Licence.

internalization of nanoparticles and bacteria by multi-spectral imaging flow cytometry, *J. Visualized Exp.*, 2012, (64), e3884.

45 M. J. Munro, S. T. Tan and C. Gray, Applications for Colon Organoid Models in Cancer Research, *Organoids*, 2023, **2**(1), 37–49.

46 B. Laperrousaz, S. Porte, S. Gerbaud, V. Härmä, F. Kermarrec, V. Hourtane, F. Bottausci, X. Gidrol and N. Picollet-D'hahan, Direct transfection of clonal organoids in Matrigel microbeads: a promising approach toward organoid-based genetic screens, *Nucleic Acids Res.*, 2018, **46**(12), e70–e70.

47 L. Wasungu, J. M. Escoffre, A. Valette, J. Teissie and M. P. Rols, A 3D in vitro spheroid model as a way to study the mechanisms of electroporation, *Int. J. Pharm.*, 2009, **379**(2), 278–284.

This journal is © The Royal Society of Chemistry 2024